American Mineralogist, Volume 75, pages 477–489, 1990

Crystal structure determinations of synthetic sodium, magnesium, and potassium birnessite using TEM and the Rietveld method

Jeffrey E. Post
Department of Mineral Sciences, Smithsonian Institution, Washington, D.C. 20560, U.S.A.
David R. Veblen
Department of Earth and Planetary Science, The Johns Hopkins University, Baltimore, Maryland 21218, U.S.A.

Abstract

The Rietveld method and electron diffraction have been used to determine, for the first time, the crystal structures of the subcells of synthetic Na-, Mg-, and K-rich birnessite-like phases. The subcells have $C2/m$ symmetry and unit-cell parameters: Na: $a = 5.175(1)$ Å, $b = 2.850(1)$ Å, $c = 7.337(3)$ Å, $\beta = 103.18°$; Mg: $a = 5.049(1)$ Å, $b = 2.845(1)$ Å, $c = 7.051(1)$ Å, $\beta = 96.65(1)°$; K: $a = 5.149(2)$ Å, $b = 2.843(1)$ Å, $c = 7.176(3)$ Å, $\beta = 100.76(3)°$. The general birnessite structure is analogous to that of chalcophanite. Difference-Fourier analyses combined with Rietveld refinements show that the water molecules and interlayer cations occupy different positions in the three birnessite structures. Electron-diffraction patterns reveal different superstructures that probably arise from ordering of interlayer water molecules and cations for each of the three phases.

Introduction

Birnessite is a member of the family of manganese oxide minerals that have layer structures (phyllomanganates). It was first described as a natural phase from Birness, Scotland, by Jones and Milne (1956), and they reported the chemical formula $(Na_{0.7}Ca_{0.3})Mn_7O_{14} \cdot 2.8H_2O$. It is now recognized that birnessite and birnessite-like minerals occur in a wide variety of geological settings. Birnessite is a major Mn phase in many soils (Taylor et al., 1964; Chukhrov and Gorshkov, 1981; Cornell and Giovanoli, 1988) and an important component in desert varnishes (Potter and Rossman, 1979a) and ocean manganese nodules (Burns and Burns, 1976). Birnessite also is commonly found as an alteration product in Mn-rich ore deposits. Recent studies have shown that birnessite readily participates in cation-exchange and oxidation-reduction reactions (e.g., Oscarson et al., 1981) and therefore might play a significant role in soil and ground-water chemistry. Birnessite is also one of the phases reported from bacterially precipitated Mn oxides (K. Mandernack, personal communication).

Despite the large volume of work that has been published about birnessite and the phyllomanganates in general, little is known about the details of the crystal structure of birnessite. All of the known natural and synthetic birnessite samples are extremely finely crystalline or poorly ordered or both, and to date no crystals have been found that are suitable for single-crystal diffraction studies. Even the crystal system and the unit cell for birnessite have been subjects of speculation. In this study, we have used the Rietveld method and powder X-ray diffraction data, along with transmission electron microscopy (TEM) and selected-area electron diffraction (SAED), to solve and refine for the first time the crystal structures of three synthetic birnessite phases.

Based on its typically platy crystal morphology, as viewed with a TEM, and the similarity of its powder X-ray diffraction pattern to that of chalcophanite, it has long been assumed that birnessite has a layer structure. Chalcophanite is constructed of layers of edge-sharing Mn^{4+}-O octahedra, in which one of seven Mn sites is vacant, separated by a layer of water molecules (Fig. 1). Zinc cations occupy sites above and below the Mn vacancies and are in octahedral coordination with three oxygen atoms each from the Mn and water layers (Wadsley, 1955; Post and Appleman, 1988). Burns and Burns (1977) proposed that the structure of birnessite is analogous to that of chalcophanite but with Na or Ca, etc., replacing the Zn cations. Combining TEM and EX-AFS (Crane, 1981) data from synthetic birnessites, Giovanoli and Arrhenius (1988) suggested a birnessite structure in which one of six layer Mn sites is vacant and various 2+ and 3+ interlayer cations occupy positions above and below the vacancies. The interlayer region also contains water molecules and water-coordinated cations such as Na^+. Some OH^- replaces O^{2-} as needed for charge balance. Giovanoli et al. (1970) proposed an orthorhombic unit cell for synthetic Na-bearing birnessite, based on electron diffraction patterns, with $a = 8.54$ Å, $b = 15.39$ Å, and $c = 14.26$ Å. Cornell and Giovanoli (1988) were not able, however, to index diffraction patterns from synthetic K-rich birnessite using this unit cell.

Chukhrov et al. (1985) used powder X-ray diffraction patterns from natural birnessite (dredged from the ocean floor) to test two birnessite models based on the chalcophanite structure. The model that yielded the best fit

0003–004X/90/0506–0477$02.00

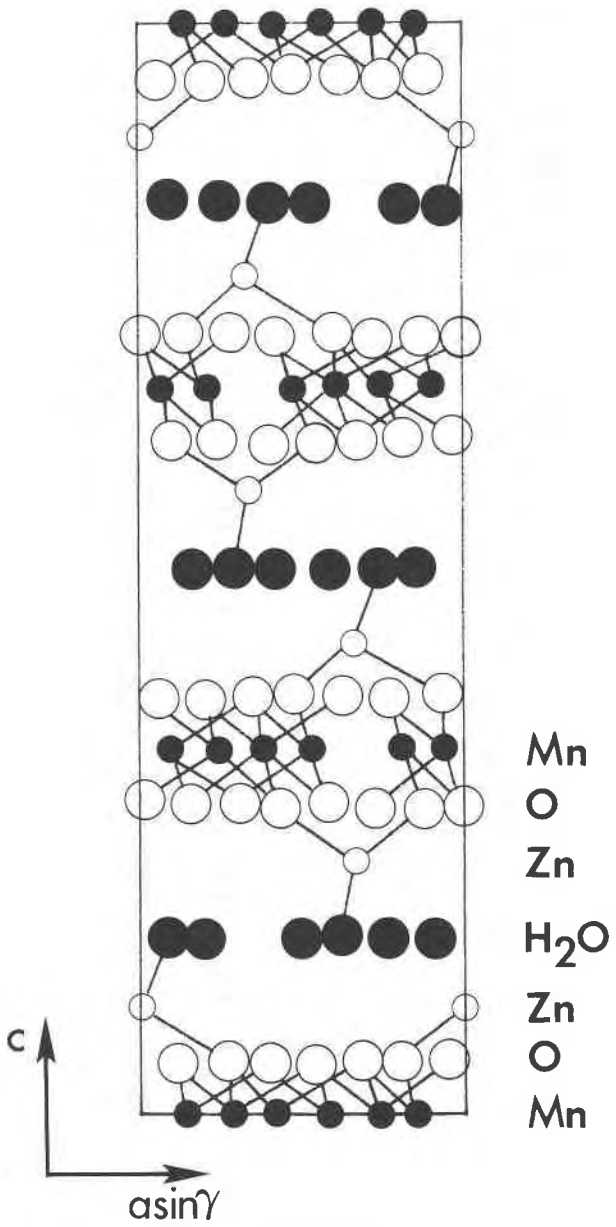

Fig. 1. Projection of the chalcophanite structure along **a** (after Post and Appleman, 1988).

between the observed and calculated patterns (using the model structure) had Mn vacancies randomly distributed in the Mn-O octahedral layers and Na cations above and below the vacancies. They reported a hexagonal unit cell for birnessite with $a = 2.86$ Å and $c = 7$ Å.

Experimental

Following the example of many previous investigators, we have used synthetic birnessite phases in our studies because they are in general better structurally ordered than the natural material. Also, the synthetic phases have simpler compositions than natural birnessites, therefore reducing the complexity of the crystal-structure study. The Na-rich birnessite-like phase (Na-birn) was synthesized by D. C. Golden using a modification of the procedure of Stähli (1968) (Golden et al., 1986). A K-rich birnessite-like phase (K-birn) was prepared by shaking a sample of the Na-birn in 1 M KCl solution for 12 h (Golden et al., 1986), and a Mg-rich birnessite-like phase (Mg-birn) was prepared by a similar cation-exchange procedure, using 1 M $MgCl_2$, but from a different, but compositionally identical, parent Na-birn sample. Energy-dispersive X-ray analysis using the TEM confirmed that all of the Na had been replaced by Mg and K, respectively. Flame photometry, atomic absorption, and water (Penfield method) analyses, performed as part of this study, yielded the following chemical formulae for the Na- and Mg-birn:

$$Na_{0.58}Mn^{4+}_{1.42}Mn^{3+}_{0.58}O_4 \cdot 1.5H_2O \text{ and}$$
$$Mg_{0.29}Mn^{4+}_{1.42}Mn^{3+}_{0.58}O_4 \cdot 1.7H_2O.$$

The formulae are for the contents of the $C2/m$ subcell that is described below. The Mn oxidation states were assigned to give analysis totals of 100 wt%. Alternatively, one can assume all Mn^{4+} and some Mn vacancies (approximately one out of every 16 Mn sites), giving the formulae:

$$Na_{0.54}Mn^{4+}_{1.87}O_4 \cdot 1.4H_2O \text{ and}$$
$$Mg_{0.27}Mn^{4+}_{1.87}O_4 \cdot 1.6H_2O.$$

It is also possible of course that both Mn^{3+} and Mn vacancies occur in the samples. It is noteworthy that the quantities of Mn^{3+} or Mn vacancies for both birnessite samples almost exactly offset the charges of the interlayer cations (assuming no Mn in the interlayer region). Furthermore, the total interlayer-cation charge is nearly the same for the Na- and Mg-birn, suggesting that the Mn-layer charge probably did not change during the Na-Mg exchange reaction. The composition of the Na-birn used in this study agrees closely with that reported by Giovanoli et al. (1970).

We did not have a sufficient amount of K-birn to perform a water analysis, but flame-photometry analysis yielded 8.7 wt% K, and this is close to the value of 8.2 wt% K determined by J. N. Moore, J. R. Walker, and T. H. Hayes (unpublished results) for a synthetic K-bearing birnessite-like phase. The composition of their material yields the formulae $K_{0.46}Mn^{4+}_{1.6}Mn^{3+}_{0.4}O_4 \cdot 1.4H_2O$ or $K_{0.46}Mn^{4+}_{1.9}O_4 \cdot 1.4H_2O$, which are probably representative of our K-birn sample.

Samples of each of the three synthetic birnessites were dispersed in alcohol and suspended onto holey-carbon grids for TEM examination using a Philips 420ST electron microscope operated at 120 KeV. The crystallites in all three samples show the typical pseudo-hexagonal, platy morphology (Fig. 2) that has been observed for birnessites by previous investigators (e.g., Giovanoli et al., 1970; Chukhrov et al., 1985; Chen et al., 1986; Cornell and Giovanoli, 1988). Also, as previously reported, many of the crystals are twinned (Fig. 2). Typically the crystallites

measure about 2 μm across the plate and are approximately 250–600 Å (Na- and K-birn) or 1000–2000 Å (Mg-birn) thick. The TEM examination also revealed the presence of a small amount of hausmannite as an impurity in the Na- and K-birn samples (Fig. 2).

SAED patterns for all three phases corresponding to the direction normal to the plates show similar pseudo-hexagonal arrangements of strong subcell reflections (Fig. 3). Also apparent in the diffraction patterns, however, are weaker reflections arising from superstructures that are different for the three birnessite phases. The superstructure reflections exhibit a range of intensities for different crystals and in some cases are absent. Streaking associated with super- and substructure reflections is obvious in nearly all of the patterns, suggesting some type of structural disorder. Like the discrete superlattice reflections, the streaking is variable from crystal to crystal, and some diffraction patterns also exhibit diffuse spots of intensity.

In addition to the Na-, Mg-, and K-birn phases described, we performed electron diffraction, analytical TEM (AEM), and high-resolution TEM experiments on an aliquot of the K-birn sample that had been allowed to age in impure alcohol in a glass vial (Baker analyzed reagent anhydrous alcohol #9401-3). The AEM analyses of this material showed that approximately half of the K had been replaced by Na. SAED patterns showed superstructures similar to those for pure Na-birn, but with less streaking of the superstructure diffraction spots than shown by the other samples (Fig. 3d). The relatively well-ordered superstructure implied by the SAED patterns presumably resulted from ordering that occurred during the prolonged immersion in alcohol. Lattice images show the superstructure to be well-ordered on average (Fig. 4), but with occasional defects such as out-of-phase boundaries.

It was possible to tilt some of the crystals such that diffraction patterns and high-resolution structure images could be recorded looking parallel to the plate direction (Fig. 5). The diffraction patterns in this orientation are generally not of high quality and typically show only substructure spots, but they do provide important information about interplanar spacings normal to the plates and about the symmetry of the subcell. The structure image and diffraction pattern in Figure 5, taken parallel to the plate, indicate that the Na-birn structure has collapsed in the vacuum of the microscope from an interlayer spacing of about 7 Å (as measured from powder X-ray diffraction patterns obtained under ambient conditions) to approximately 5 Å. Presumably, this collapse corresponds to the loss of the interlayer water. The interlayer spacings for K-birn decreased only slightly in the TEM, to between 6.0 and 7.0 Å, but more severe collapse was observed near the edges of some crystals (Fig. 6). No collapse was observed for Mg-birn. Computer simulations of high-resolution TEM images by Guthrie (1989) indicate that the dark fringes in Figures 5a and 6, recorded at optimum defocus, correspond to the Mn-O layers.

Comparison of d-values measured from powder X-ray and electron diffraction patterns for Na-, K-, and Mg-birn indicate that only reflections corresponding to the strong substructure spots on the electron-diffraction patterns are observed in the X-ray diffraction patterns. This is the case even for X-ray diffraction (XRD) patterns obtained using long counting times (20 s/step). This is consistent with the observation that a large number of the possible diffraction lines calculated using the unit cell proposed by Giovanoli et al. (1970) for Na-birn, which was derived using both super- and subcell reflections in electron-diffraction patterns, do not appear in experimental birnessite powder XRD patterns. Because XRD data contain minimal information about the superstructures, we have focused in this study on the birnessite substructures.

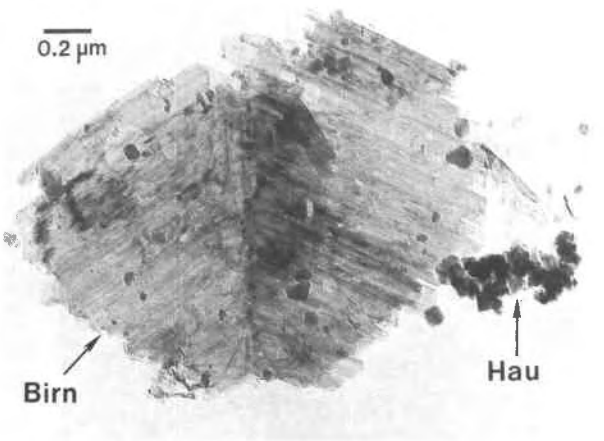

Fig. 2. TEM image of a typical twinned plate of Na-birn (Birn). Also shown are some crystals of hausmannite (Hau), which occurs as a minor impurity.

We were not able to index the synthetic birnessite XRD patterns using any of the previously reported birnessite unit cells. The arrangement of substructure spots on the electron-diffraction patterns for Na-birn in Figure 3 suggested the possibility of a C-centered monoclinic unit cell. Independently, we attempted to index the powder XRD pattern for Na-birn using the computer program TREOR (P. E. Werner, personal communication). All of the non-hausmannite peaks in the pattern were successfully indexed only on a C-centered unit cell with dimensions that were almost exactly the same as those measured from the electron diffraction patterns (Table 1). Both the XRD and electron diffraction data, then, indicate a subcell with space-group symmetry $C2/m$, Cm, or $C2$. We arbitrarily selected the centrosymmetric space group $C2/m$. Starting with the unit cell for Na-birn, we were subsequently able to index the patterns and refine unit cells for Mg- and K-birn (Table 1).

Powder XRD data for Rietveld analysis were collected for the three synthetic birnessite samples with Cu $K\alpha$ radiation using a Scintag automated powder X-ray diffractometer outfitted with incident- and diffracted-beam Soller slits and an intrinsic-Ge solid-state detector. Count times ranging between 16 and 20 s per 0.03° step were

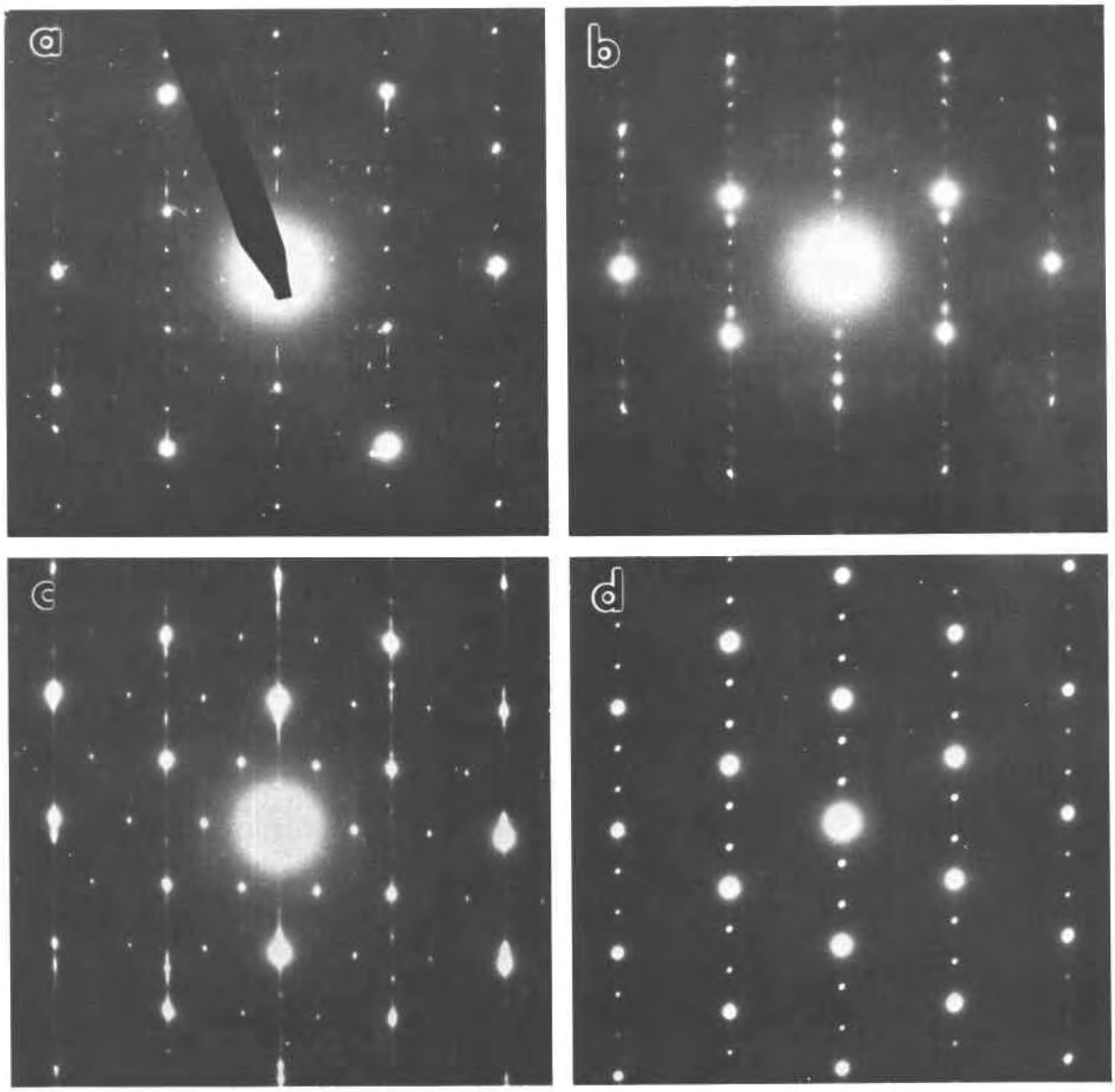

Fig. 3. Selected-area electron-diffraction patterns obtained with the electron beam parallel to the *c*-axis. The *a**-axes are vertical, and the *b**-axes are horizontal. (**a**) Na-birn. (**b**) Mg-birn. (**c**) K-birn. (**d**) Aged K/Na-birn.

used over the 2Θ range 6–90°. There are no obvious reflections above 90° 2Θ, probably because of structural disorder in the samples. Because of the small crystallite sizes revealed by TEM for the birnessites, the samples were only lightly ground under acetone. The Mg-birn was packed into an Al cavity mount, and in an attempt to minimize any preferred orientation effects, the Na- and K-birn samples were sieved onto glass-fiber filters for data collection. The low-angle portion of each data set (<23° 2Θ) was excluded during refinement because in this region not all of the incident X-ray beam strikes the sample, and therefore relative observed intensities are too low.

Refinement

Because the Rietveld method is generally a refinement technique and is not well-suited for solving structures, it was necessary to develop at least a partial starting crystal-structure model for birnessite. We used the Mn-O octahedral layer in chalcophanite (Post and Appleman, 1988) as a model for the Mn-O layer in birnessite. The chemical analyses and unit-cell information indicated approximately two Mn atoms per cell, and these were assigned to special position 2a of space group $C2/m$. The starting octahedral O atom was placed by analogy to chalcopha-

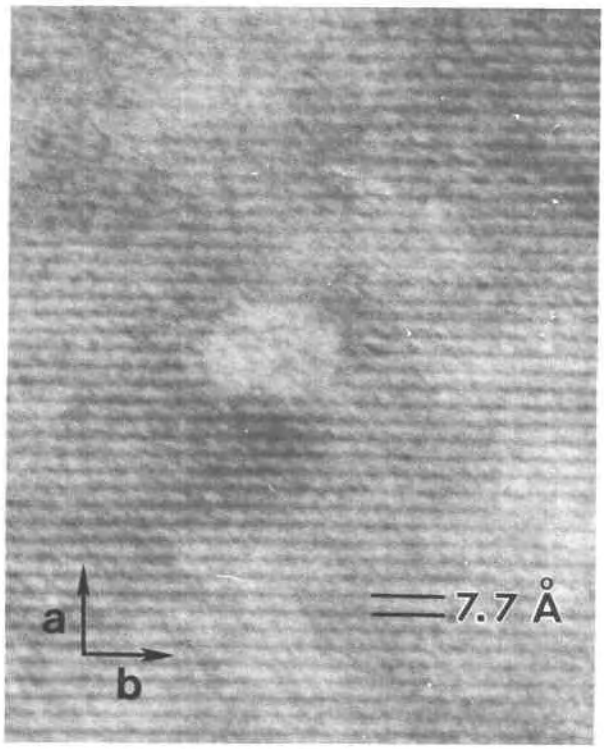

Fig. 4. High-resolution TEM image showing fringes arising from the well-ordered 7.7 Å superstructure in aged K/Na-birn.

nite. No interlayer cations or water molecules were included in the starting structure model.

The Rietveld refinements were carried out using the computer program DBW3.2 as modified by S. Howard (personal communication). During the initial cycles of Rietveld refinement, using the birnessite structure model described above, only the scale factor, background and profile-shape coefficients, unit-cell parameters, and sample-displacement correction factor were refined. The background was fit using a third-order polynomial, and the observed peak shapes were approximated with a pseudo-Voigt profile function, limited to six full-widths on each side of the peak maximum.

TABLE 1. Final Rietveld refinement parameters

	Na-birn	Mg-birn	K-birn
a (Å)	5.174(1)	5.050(1)	5.149(2)
b (Å)	2.850(1)	2.846(1)	2.843(1)
c (Å)	7.336(3)	7.054(1)	7.176(3)
β (°)	103.18(2)	96.63(1)	100.76(3)
V (Å^3)	105.3	100.7	103.0
Pseudo-Voigt coefficient	0.70(4)	1.22(3)	1.15(3)
Overall B	1.4(2)	1.3(1)	−0.7(3)
R_{wp}	0.115	0.148	0.115
R_{wp} (expected)	0.074	0.106	0.084
R_B	0.085	0.091	0.091

Na-birn

After the initial stage of refinement described above, the values of R_{wp} and R_B for Na-birn were 0.17 and 0.23, respectively, suggesting that the model was a reasonable approximation of the Mn-O layer portion of the birnessite structure. As mentioned above, there is a small amount of hausmannite mixed with the Na- and K-birn samples. Therefore, hausmannite was included in the refinement, and its unit-cell parameters, scale factor, and peak widths were refined, lowering R_{wp} to 0.16. The refinement determined that the Na-birn sample contains approximately 2 wt% hausmannite.

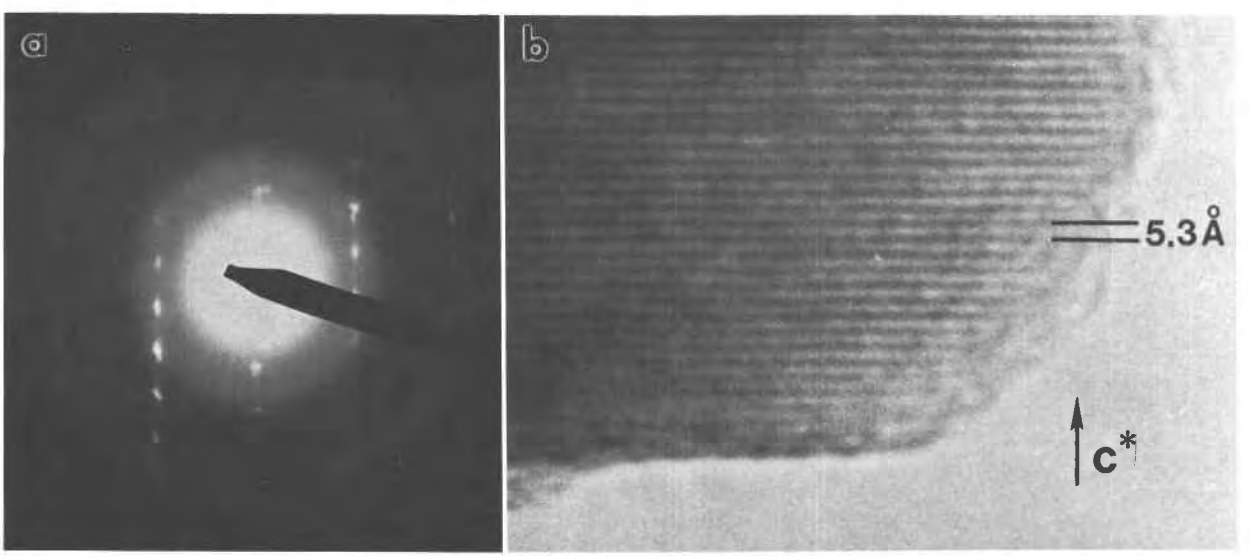

Fig. 5. (**a**) Selected-area electron-diffraction pattern and (**b**) high-resolution TEM image obtained from Na-birn with the electron beam parallel to the layers. This structure collapses in the vacuum of the electron microscope from an interlayer spacing of 7.1 Å to approximately 5 Å.

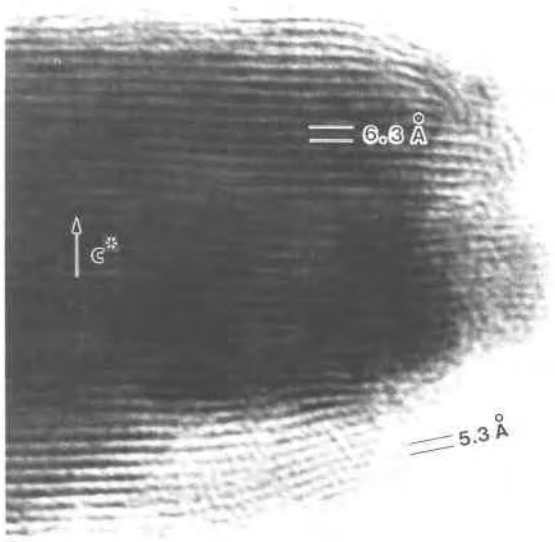

Fig. 6. High-resolution TEM image showing layering in K-birn. Most of the layers in this structure collapse in the electron microscope to a spacing between 6 and 7 Å, but some of the material at the very edges of the plates collapses to about 5 Å.

In an attempt to locate the positions of the interlayer Na cations and water molecules, difference-Fourier maps were calculated using the observed Bragg intensities resulting from the Rietveld refinement procedure described above. These intensities were corrected for multiplicity and Lorentz-polarization effects and converted into structure factors for use in the XTAL crystallographic computing package (Stewart and Hall, 1985). Using the same partial birnessite structure model as above, an overall scale factor was refined, and a three-dimensional difference-Fourier map was calculated (Fig. 7).

TABLE 2. Synthetic birnessite atomic parameters

		x	y	z	Occ*
Mn	Na	0	0	0	
	Mg	0	0	0	
	K	0	0	0	
	Ch	0	0	0	
O1	Na	0.376	0	0.133	
	Mg	0.356	0	0.141	
	K	0.365	0	0.136	
	Ch	0.28	0	0.15	
O2	Na	0.595	0	0.500	2.0
	Mg	0.703	0	0.506	1.5
	K	0.723	0	0.522	1.3
	Ch	½	0	½	
O3	Na	0	0	½	0.3
	K	0	0	½	0.3
Mg	Mg	0.023	0	0.282	0.5
	Ch**	0.099	0	0.304	

Note: Na, Mg, and K indicate Na-, Mg-, and K-birn, respectively; Ch indicates chalcophanite *C*2/*m* subcell (Wadsley, 1955). Calculated estimated standard deviations for atom positions are 0.001 for Mn and O1, and 0.003 for O2 and Mg. Calculated estimated deviation for occupancies is about 0.05 atoms/cell. Temperature factors fixed to B = 0.5 (Mn,Mg), 1.0 (O), and 1.5 (water O).

* Occupancy factors are atoms/unit-cell.

** Zn position for chalcophanite monoclinic subcell.

TABLE 3. Bond distances (Å) for synthetic birnessites

	Na-birn	Mg-birn	K-birn
Mn-O1 (×4)	1.92	1.92	1.92
-O1 (×2)	1.97	1.97	1.95
Mean	1.94	1.94	1.93
O1-O1 (×2)	2.53	2.54	2.52
-O1	2.57	2.62	2.59
-O2	2.66	2.60	2.57
-O2	2.67	2.88	3.02
-O1 (×2)	2.85	2.85	2.84
-O1 (×4)	2.95	2.94	2.94
-O3 (×2)	2.98		2.93
O2-O2 (×2)	2.15	1.51	1.49
-O2	0.98	2.08	2.26
-O2 (×2)	2.85	2.84	2.84
-O2 (×4)	2.95	2.94	2.94
-O2	3.02	3.08	2.93
Mg-O1 (×2)		1.86	
-O2		2.50	
-O1		2.15	
-O2 (×2)		2.18	
Mean		2.13	

Note: Calculated estimated standard deviations are 0.01 Å for Mn-O and 0.03 Å for Mg-O and O-O distances.

When interpreting difference maps based on Rietveld intensities, it is important to consider that the results are biased by the model structure, and consequently the amount of information on the maps is typically less than on comparable maps resulting from single-crystal data. Even so, Post and Bish (1988) used combined Rietveld and Fourier analysis to successfully locate cavity species in todorokite and analcime. The dominant feature on the difference map calculated for Na-birn (Fig. 7A) is an electron density peak (1.9 $e^-/Å^3$) at (0, ½, ½), and there are no other peaks in the interlayer region of the map larger than 0.8 $e^-/Å^3$. Because most of the electron density in the interlayer region of Na-birn is due to water, it is likely that the largest difference peak indicates a water site, and an O atom at (0, ½, ½) was included in the Na-birn structure model. The refinement yielded a water (O2) position at (0.59, 0, 0.50) with an occupancy factor equivalent to about 2.0 H_2O/cell, and R_{wp} decreased to 0.14 and R_B to 0.13. At this point a second difference-Fourier map was calculated, and it showed an electron density peak (1.1 $e^-/Å^3$) in the interlayer region at (½, ½, ½). An O atom (O3) was included in the Rietveld refinement at this site and its occupancy factor refined, resulting in R_{wp} and R_B dropping to 0.12 and 0.11, respectively. In the final stages of the refinement, all of the atomic positional parameters not fixed by symmetry and occupancy factors for the interlayer sites were allowed to vary. Individual temperature factors were held fixed to the comparable values determined by Post and Appleman (1988) for chalcophanite, and an overall temperature factor was refined.

Mg- and K-birn

The refinements of the Mg- and K-birn structures were carried out following the same procedures as described

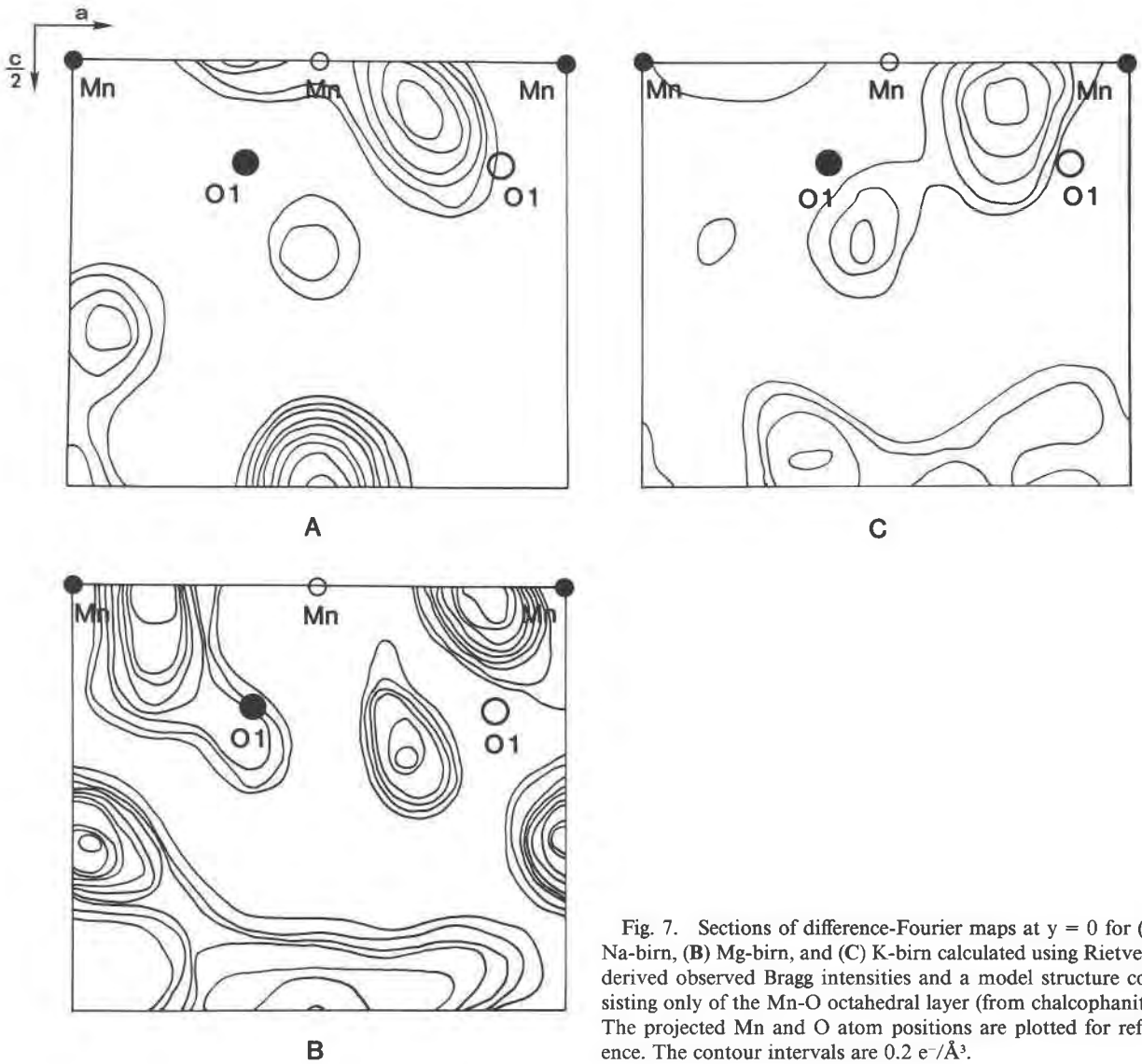

Fig. 7. Sections of difference-Fourier maps at y = 0 for (**A**) Na-birn, (**B**) Mg-birn, and (**C**) K-birn calculated using Rietveld-derived observed Bragg intensities and a model structure consisting only of the Mn-O octahedral layer (from chalcophanite). The projected Mn and O atom positions are plotted for reference. The contour intervals are 0.2 $e^-/Å^3$.

above for Na-birn. The difference-Fourier map calculated for Mg-birn showed two significant electron density peaks in the interlayer region (Fig. 7B). A large, diffuse peak centered at about (½, 0, ½) was assumed to correspond to the water site, and a second smaller peak at about (0, 0, 0.31) to the Mg position. The Rietveld refinement yielded a water position for Mg-birn at (0.70, 0, 0.5). For Mg-birn we attempted to refine individual isotropic temperature factors for Mn, O1 and O2 (water) atoms, and all values were quite large: Mn(B) = 3.5, O1(B) = 1.8, and O2(B) = 12. In Rietveld refinements, temperature factors may accommodate a range of errors in the structure model, and therefore commonly are unreliable. If at all realistic, however, the large B values refined for Mg-birn indicate considerable positional disorder, especially on the water site. The difference map for K-birn (Fig. 7C) revealed a single diffuse interlayer electron-density peak centered at (½, 0, ½), and apparently both the K and water occupy this site. The refined K/H_2O position is at about (0.72, 0, 0.52). Final observed and calculated profiles for the three birnessite refinements are compared in Figure 8. The final residuals and atomic parameters are listed in Tables 1 and 2, respectively, and selected bond distances are listed in Table 3. The crystal structures of Na- and Mg-birn are illustrated in Figure 9.

In the cases of Na- and Mg-birn, we also completed structure refinements using integrated Bragg intensities measured from the powder XRD patterns using a Pearson VII profile function and an algorithm supplied with our Scintag diffractometer system. The intensities for 27 (Na-

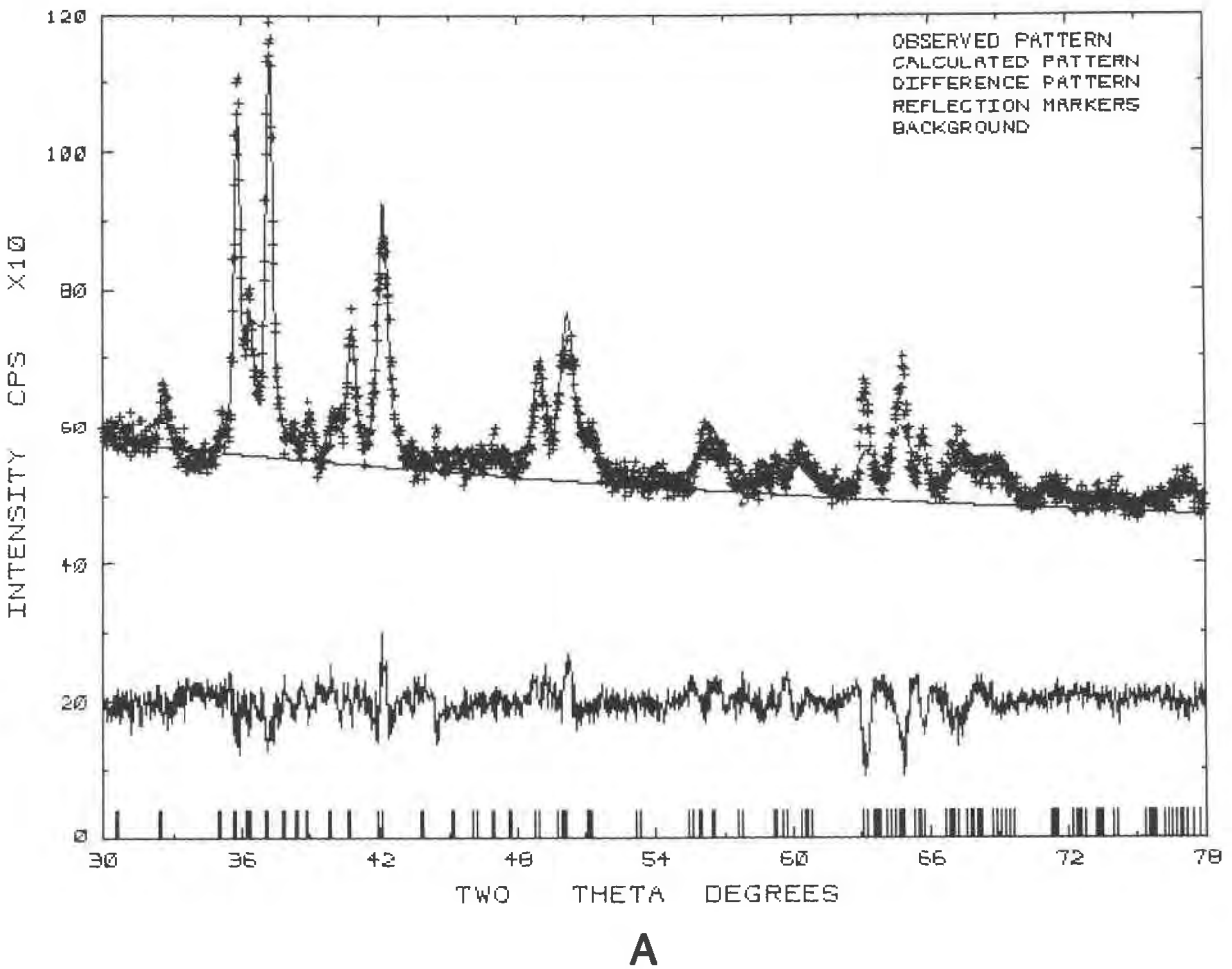

Fig. 8. (A) Final observed (crosses), calculated, and difference powder XRD patterns for Na-birn + hausmannite. The background is indicated by the horizontal line, and the vertical lines mark the positions of the Bragg reflections ($K\alpha_1$ and $K\alpha_2$).

birn) and 22 (Mg-birn) Bragg reflections were corrected for Lorentz, polarization, and multiplicity effects and converted to structure factors for use in the XTAL package. Difference-Fourier maps, calculated using the same Mn-O layer model as for the Rietveld refinements, are very similar to those determined using the Rietveld intensities. Refinements of the atomic parameters (not including temperature factors) using the peak-fitting data resulted in residuals of 0.12 (Na-birn) and 0.13 (Mg-birn) and yielded parameter values within estimated standard deviations of the Rietveld values.

Discussion

The refinement results are consistent with a layer structure for synthetic birnessite similar to that of chalcophanite. In fact, the final atom positions for the three birnessite structures agree quite well with those reported by Wadsley (1955) for a monoclinic subcell of chalcophanite (Table 2). The chalcophanite monoclinic subcell can be transformed into a trigonal unit cell (Post and Appleman, 1988), but such is not the case for birnessite. Unfortunately, it is difficult to assess the accuracy of our refined birnessite atom positions and, consequently, bond distances. The estimated errors determined by the Rietveld refinements are based on counting statistics in the data but do not account for systematic errors in the profile functions nor for sample-related problems such as preferred orientation and structural disorder. Replicate XRD data sets collected for our synthetic birnessite samples do not show evidence of significant preferred orientation problems; however, the possibility of minor effects cannot be dismissed.

A more serious problem encountered in our refinements is that the Bragg peaks in the birnessite powder patterns show pronounced anisotropic broadening and therefore are not well described by the relatively simple peak-width function in the Rietveld refinement program DBW. This broadening is caused by two major factors: 1) small sizes and anisotropic shapes (i.e., plates) of the birnessite crystallites, and 2) structural disorder in certain

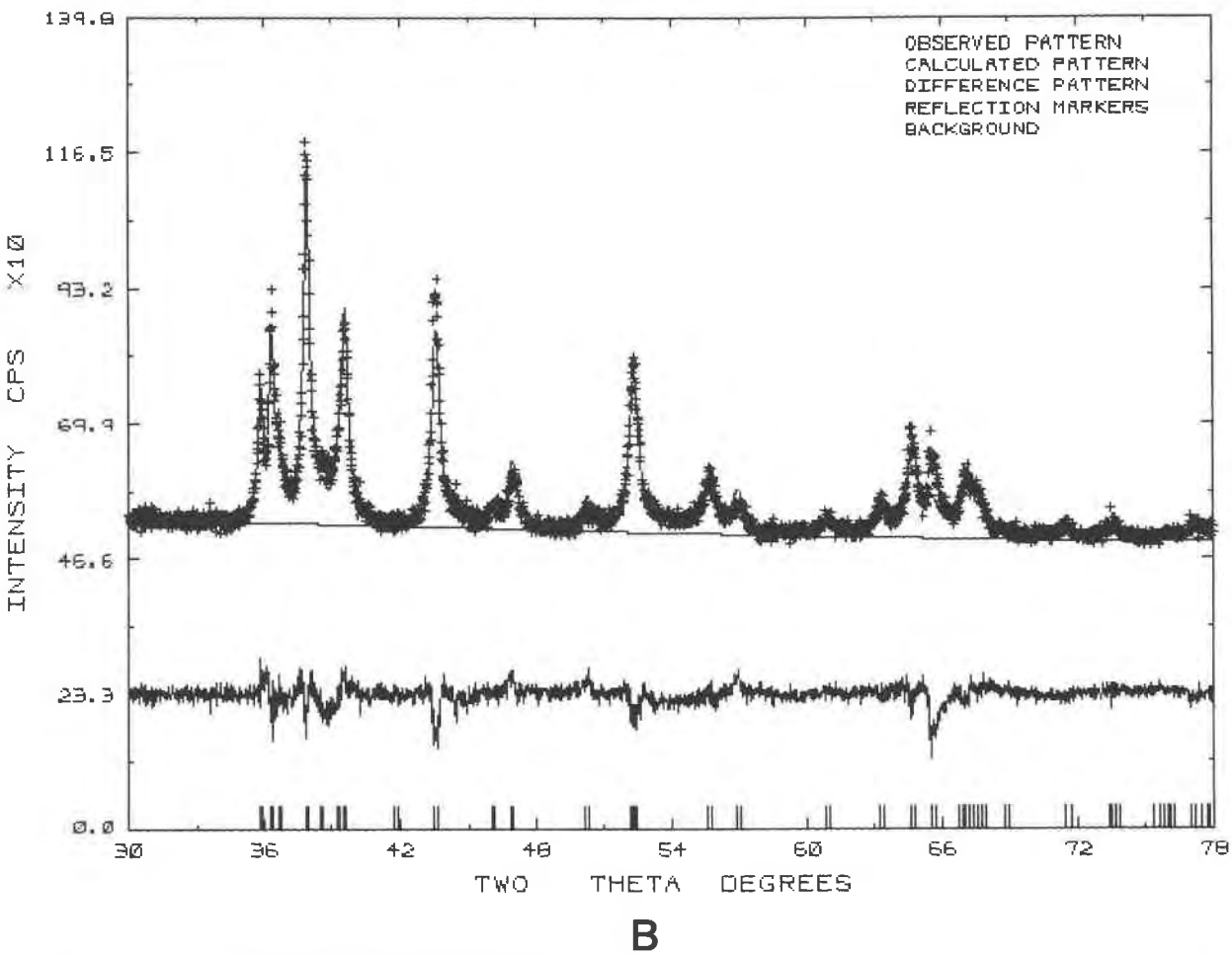

Fig. 8.—*Continued.* (**B**) Final observed (crosses) calculated, and difference powder XRD patterns for Mg-birn. See also Figures 8A and 8C.

crystallographic directions. Particle size and shape effects should broaden the (001) reflections (the *c* crystallographic direction in birnessite corresponds to the thin particle dimension) in the birnessite powder XRD patterns relative to other reflection classes. Although all of the peaks in the birnessite patterns are broad, the greatest degree of broadening is exhibited not by the (001) but rather by the (111) reflections. This is consistent with the streaking observed along the (110) direction in the birnessite electron-diffraction patterns and suggests that much of the observed peak broadening is caused by structural disorder. Most of the differences between the observed and calculated birnessite patterns in Figure 8 result from having used a single average peak-width function. The magnitude of the impact of the peak-width-fitting problem on the refined structures is not known. A study by Greaves (1985), however, concluded that improper modeling of anisotropic peak widths typically has little effect on the refined atomic positional parameters. This is reinforced by the good agreement between our Rietveld Na- and Mg-birn atomic parameters and those determined using peak-fitting data.

Octahedral layer

The average Mn-O bond distances for Na-, K-, and Mg-birn (Table 3) are only slightly larger than the value of 1.906 reported for chalcophanite (Post and Appleman, 1988). Because of the uncertainties in our refined bond distances, it is not possible to know if this difference is significant. It is possible, however, that the larger birnessite Mn-O distances result from a small amount of Mn^{3+} (Mn^{3+}-O distance $\approx$ 2.01 Å) substituting for Mn^{4+}. Refinements of the Mn occupancy factors for each of the three birnessite structures yielded values that are not significantly different from 1.0, indicating that the fraction of vacancies on the Mn sites, if any, is small. As discussed above, the interlayer cation charges are offset by either Mn^{3+} or vacancies, or both, in the Mn octahedral layer. Unfortunately in the cases of the birnessites used in this study, the quantities of either Mn^{3+} ($\approx$25% of the total

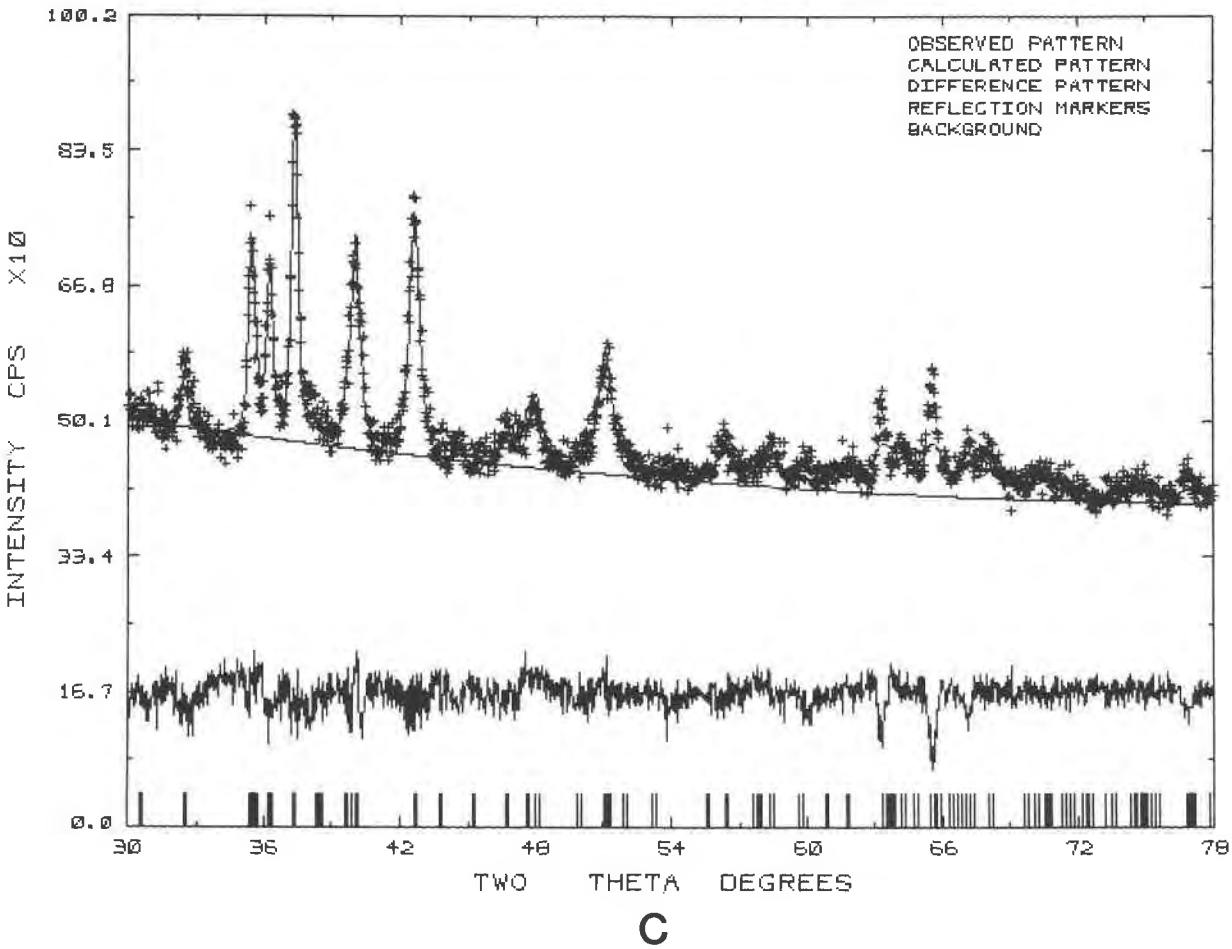

Fig. 8.—*Continued.* (C) Final observed (crosses), calculated, and difference powder XRD patterns for K-birn + hausmannite. See also Figures 8A and 8B.

Mn) or vacancies (≈7% of the total Mn) required to maintain charge-balance are small, and it is not possible from our refinements to distinguish between the two charge-compensating mechanisms. It is interesting, but perhaps fortuitous, that the mean Mn-O distances in Table 3 are very close to the expected value for Mn sites having 25% Mn^{3+} and 75% Mn^{4+}. The highly oxidizing conditions of the birnessite syntheses, however, would tend to argue against significant amounts of Mn^{3+} in the birnessite structures.

Interlayer species

The predominant interlayer species, according to the chemical analyses, for the three birnessite samples is water. In Na-birn the difference-Fourier analysis and subsequent Rietveld refinements indicate a partially occupied water (O2) site at about (0.59, 0, ½). The refined occupancy (Table 2), corresponding to approximately 2.0 H_2O/cell, is greater than the 1.4 to 1.5 H_2O/cell determined by chemical analysis but is close to the expected value for total Na and H_2O. The diffuseness of the electron-density peak at the O2 site on the difference map for Na-birn is likely evidence of positional disorder. The disorder might be caused by Na and H_2O occupying different sites within a unit cell and a range of positions in different unit cells, depending, for example, on whether or not the particular cell contains a Na cation. Several bond distances in the range 2.7–2.96 Å between O2 atoms, and between O2 and O1 in the Mn-O octahedral layer, suggest possible hydrogen bonds. The difference map for Na-birn indicated a second possible interlayer site (O3) at (0, 0, ½). The refined occupancy factor corresponds to about 0.4 O atoms/cell. Again, the difference map shows extremely diffuse electron density at this site. It should be noted that it is not possible based on the results of our refinements to assign exclusively Na or H_2O to a particular interlayer site. Most likely Na and H_2O are disordered over one or both of the interlayer sites, which explains, at least in part, the positional disorder indicated by the difference map.

The difference-Fourier map and subsequent Rietveld refinement determined that the main interlayer water site

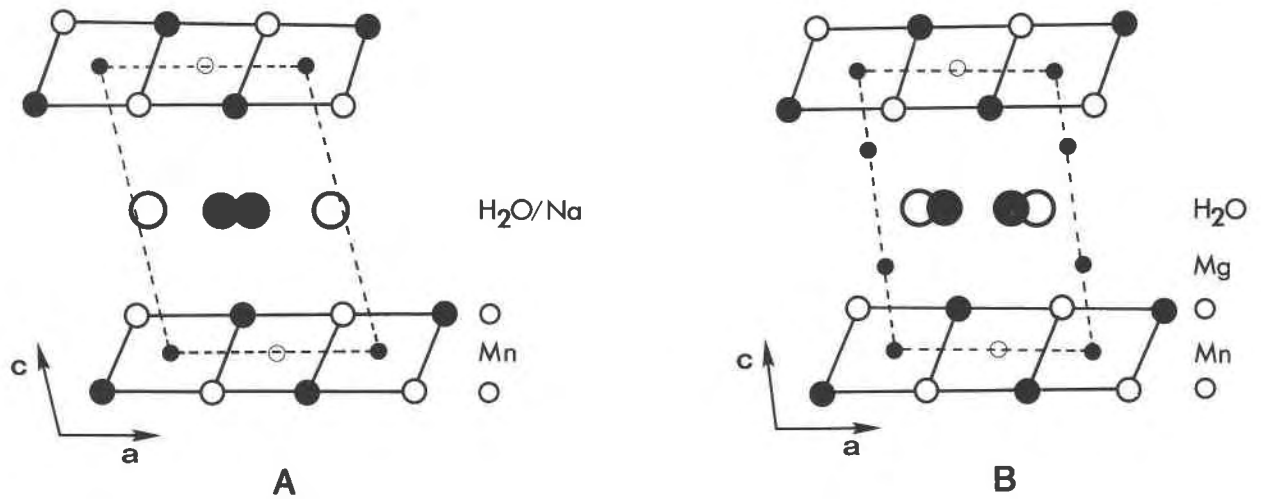

Fig. 9. Projections of the (**A**) Na-birn and (**B**) Mg-birn structures along *b*. The open circles indicate atoms at y = ½, and the solid circles indicate atoms at y = 0.

for Mg-birn is at (0.70, 0, 0.50) and is about 40% occupied (1.5 H_2O/cell). The refined occupancy is slightly less than the analytical value of 1.6–1.7 H_2O/cell. As with Na-birn, the difference map indicates the likelihood of some positional disorder over the water site in Mg-birn. Three of the calculated water-water bond distances are shorter than 2.0 Å, implying that certain neighboring water sites cannot simultaneously be occupied. The number of water molecules per Mn site determined analytically for Mg-birn is nearly the same as for chalcophanite. The water molecules in chalcophanite form a hexagonal close-packed layer with one out of seven molecules absent. The water oxygen in Mg-birn forms one obvious hydrogen bond to O1 (about 2.65 Å) in the Mn-O octahedral layer, which undoubtedly contributes to the binding force between layers. Several O2-O2 distances in the range 2.8–2.9 Å suggest other possible hydrogen bonds within the water layer.

The difference map for Mg-birn revealed a second electron density peak in the interlayer region at about (0, 0, 0.31), which is analogous to the Zn position in chalcophanite. Because Zn and Mg are comparable in size and valence, we assigned Mg to the second interlayer site in Mg-birn. The refined Mg occupancy (0.5 Mg/cell) is larger than the analytical value of about 0.3 Mg/cell. It should be noted, however, that considering the marginal quality of the XRD data (due to structural disorder in the samples), the fact that the interlayer sites are only partially occupied, and the diffuse nature of the electron density at the interlayer sites as revealed on the difference map, it is probable that all of the refined occupancy factors presented here are only gross approximations. Also, temperature and occupancy factors are typically highly correlated in structure refinements, and therefore, the fact that we have generally not refined atomic thermal parameters undoubtedly introduces some errors into the occupancy factors. In any case, the actual uncertainties in the occupancy factors are probably considerably larger than the standard deviations calculated during the Rietveld refinements. The Mg is octahedrally coordinated to three O atoms in the Mn-O layer and to three water O atoms. The average Mg-O bond length of 2.13 Å is slightly larger than the predicted Mg-O distance of 2.08 Å (Shannon, 1976). The range of individual Mg-O bonds (1.88–2.40 Å) is greater than that typically observed in other structures and probably is the result of positional disorder, which makes it difficult to determine actual Mg-O bond lengths.

The structure refinement of K-birn indicates that the water molecules and K atoms both occupy an interlayer site at about (0.72, 0, 0.50). No other significant electron-density peaks are observed in the interlayer region on the difference map. The refined occupancy factor for the H_2O/K position is approximately 75% of the expected value, assuming the chemical formula given above. The occupancy factor increases with the value of the assigned temperature factor, and considering the diffuseness of the electron density over the interlayer site (Fig. 7C), both our assigned temperature factor (B = 2) and consequently the refined occupancy are too small. As in Mg- and Na-birn, the short distances between some of the interlayer water-cation sites imply that certain adjacent sites cannot simultaneously be occupied. If the water molecules and K atoms have a hexagonal close-packed arrangement, as is the case for the water molecules in chalcophanite, then the distances between H_2O/K sites are in the range of 2.84–2.94 Å, which are typical values for water-water and K-O bonds. Additionally, each water molecule or K atom is about 2.6 and 3.0 Å, respectively, from two O1 atoms in the Mn-O layer. It is likely that the K atoms and water molecules each occupy slightly different positions and that the refined position represents an average. If this is the case, then, the actual water-water and K-O bond distances are probably slightly different from those reported

in Table 3. The Rietveld refinement did yield a small occupancy (0.3 O atoms/cell) for K-birn at (0, 0, ½).

Some previous studies have suggested that lower-valence Mn cations occupy interlayer sites above and below possible Mn vacancies that might be in the Mn-O layers. Because Mn^{3+} and Mn^{2+} are approximately similar in size to Mg^{2+}, it is reasonable to assume that the three cations should occupy similar positions in the birnessite structure. In the case of Mg-birn, we cannot determine if some Mn is also on the Mg site. For the Na- and K-birn, however, difference maps do not show significant electron density at the expected positions for interlayer Mn, or, for that matter, significant unaccounted-for electron-density peaks anywhere else in the interlayer regions. Furthermore, Rietveld refinements of occupancy factors for the expected interlayer Mn position yielded values not significantly different from zero. We conclude, then, at least for the birnessite phases studied here, that there is very little, if any, lower-valence Mn in the interlayer region. This conclusion is consistent with the highly oxidizing conditions used to synthesize the parent Na-birn sample.

Superstructures

As mentioned above, the electron diffraction patterns for each of the three birnessite phases show different superstructures. As noted, we plan to describe the superstructures more fully in a subsequent paper, but we discuss below some of the structural aspects of ordering in birnessite-like phases. Unfortunately, we have not been able to record electron-diffraction patterns that show well-defined superstructure reflections in orientations other than down the c direction, and therefore it is not possible to define three-dimensional supercells. Previous investigators have assumed that the superstructure reflections in birnessite electron-diffraction patterns are caused by an ordering of Mn vacancies, as is the case for chalcophanite. It is not clear, however, whether the superstructures result from Mn vacancies or from long-range ordering of interlayer species. It is unlikely that ordering of only about one vacancy out of every 15 Mn sites (as required for charge balance) can give rise to the observed superstructures, much less different superstructures for Na-, Mg-, and K-birn. It is of course possible that there are greater portions of Mn vacancies than required to balance the interlayer charges, accompanied by the replacement of an appropriate number of O^{2-} by OH^-. Potter and Rossman (1979b) interpreted infrared spectra for several natural and synthetic birnessite samples as indicating the presence of an OH^- in a specific crystallographic site and disordered water. Unfortunately, there is no obvious method for ascertaining the amount of OH^- in our birnessite samples. The presence of additional Mn vacancies or OH^- is not supported, however, by our chemical analyses or structure refinements.

The fact that each of the three birnessites exhibits a different superstructure (Fig. 3) is the most compelling evidence that the superstructures arise largely from the ordering of interlayer species. As mentioned above, our chemical analyses indicate the same layer charge for Na- and Mg-birn, yet they have very different superstructures. Also, the partial occupancies determined for the interlayer water and cation sites in the subcell are consistent with some type of ordering. The superstructure reflections for Na-birn indicate a unit cell that is at least three times as large as the subcell. As mentioned above, Giovanoli et al. (1970) have proposed an orthorhombic supercell for Na-birn with $a = 8.54$ Å, $b = 15.39$ Å, and $c = 14.26$ Å. We conclude from our electron-diffraction data, however, that the actual superstructure for Na-birn probably has monoclinic or lower symmetry. The electron-diffraction patterns for Mg-birn reveal a supercell that has a volume at least six times that of the subcell. Possibly the fact that Mg-birn has one-half the number of interlayer cations as Na-birn is a factor in giving rise to a supercell that is at least double that of Na-birn. The superlattice reflections for K-birn (Fig. 3) exhibit a pseudohexagonal arrangement corresponding to a spacing within the (hk0) plane of about 4.5 Å, possibly arising from some type of H_2O/K ordering scheme. It is likely that several ordered arrangements exist in different interlayer regions in the same crystal, and no long-range order exists along the c direction among the interlayer species. A similar disordered situation might also occur in Na- and Mg-birn.

Structural variability

Many previous studies have observed that both natural and synthetic birnessite structures can accommodate a large variety of interlayer species, and our structural studies have provided some insights on how this is accomplished. First, the wide range of unit-cell parameters determined for Mg-, Na-, and K-birn (Table 1) are evidence of the flexibility of the structural framework. The angle β, for example, ranges from over 103° in Na-birn to 96.65° in Mg-birn. Only the b parameter is relatively constant for all three phases at about 2.85 Å, which is the intralayer Mn-Mn distance. Second, the water molecules and cations in the interlayer region can occupy different positions depending upon the type of cation. Ordering among the water molecules and interlayer cations, which probably gives rise to the observed superstructures, increases the stability of a particular birnessite phase. Finally, even though chemical analyses of Mg- and Na-birn indicate that both have the same Mn-O layer charge, it is likely that if natural and synthetic birnessites formed or reacted under different redox conditions, they would exhibit a range of layer charges and, consequently, compositions.

Conclusions

Our refinements for three synthetic birnessite-like phases confirm that their structures are similar to that of chalcophanite. The major differences are (1) the birnessite structures exhibit monoclinic (subcell) or possibly lower (supercells) symmetry, whereas chalcophanite is trigonal, (2) the birnessites studied here apparently have fewer Mn vacancies in the Mn-O octahedral layers than

in chalcophanite, and if vacancies are present, they might not be ordered, and (3) interlayer cation positions are different for each of the three birnessites and for chalcophanite, suggesting that the cation positions are a function of the type of interlayer cation.

Obviously, an important question is whether the synthetic phases studied here are representative of natural birnessites. Electron and powder X-ray-diffraction patterns of the synthetic phases, in general, are quite similar to those of most natural samples. The major difference is that the powder diffraction peaks for the natural birnessites are more broadened, indicating a greater degree of structural disorder. Published chemical analyses indicate that natural birnessites typically have more than one type of interlayer cation, which likely contributes to the structural disorder. Birnessites probably exhibit a range of Mn octahedral layer charges depending upon the environment of formation and, consequently, have different numbers of interlayer cations than our synthetic phases. It is almost certainly the case that the details of many natural birnessite structures are different from our refined structures. The basic crystal structures, however, are likely quite similar. We are currently attempting to refine structures for some of the "better" crystalline natural birnessite samples.

Acknowledgments

We gratefully acknowledge D. C. Golden for supplying the synthetic Na- and Mg-birnessite samples that were prepared while he was at Texas A&M University, Joseph Nelen for performing the flame photometry, atomic absorption, and water analyses, Daphne Ross for assistance with the powder X-ray diffraction, and George Guthrie for allowing us to cite results from his computer image simulations of high-resolution TEM images of birnessite. Helpful comments were provided by reviewers S. Turner and G. Arrhenius. The X-ray diffraction was supported by a grant from the International Centre for Diffraction Data, and the electron microscopy by NSF grants EAR86-09277, EAR89-03630, and EAR83-00365.

References cited

Burns, R.G., and Burns, V.M. (1976) Mineralogy of ferromanganese nodules. In G.P. Glasby, Ed., Marine manganese deposits. Elsevier, Amsterdam.

Burns, R.G., and Burns, V.M. (1977) The mineralogy and crystal chemistry of deep-sea manganese nodules, a polymetallic resource of the twenty-first century. Philosophical Transactions of the Royal Society of London (A), 286, 283–301.

Chen, C.C., Golden, D.C., and Dixon, J.B. (1986) Transformation of synthetic birnessite to cryptomelane: An electron microscope study. Clays and Clay Minerals, 34, 565–571.

Chukhrov, F.V., and Gorshkov, A.L. (1981) Iron and manganese oxide minerals in soils. Transactions of the Royal Society of Edinburgh, 72, 195–200.

Chukhrov, F.V., Sakharov, B.A., Gorshkov, A.I., Drits, V.A., and Dikov, H.P. (1985) The structure of birnessite from the Pacific Ocean. Akademiya Nauk SSSR Izvestiya, Seriya Geologicheskaya, 8, 66–73.

Cornell, R.M., and Giovanoli, R. (1988) Transformation of hausmannite into birnessite in alkaline media. Clays and Clay Minerals, 36, 249–257.

Crane, S.E. (1981) Structural chemistry of the marine manganate minerals. Ph.D. thesis, University of California, San Diego.

Giovanoli, R., and Arrhenius, G. (1988) Structural chemistry of marine manganese and iron minerals and synthetic model compounds. In P. Halbach, G. Friedrich and U. von Stackelberg, Ed., The manganese nodule belt of the Pacific Ocean. Ferdinand Enke Verlag, Stuttgart.

Giovanoli, R., Stähli, E., and Feitknecht, W. (1970) Über Oxid-hydroxide des vierwertigen Mangans mit Schichtengitter. Helvetica Chimica Acta, 53, 209–220.

Golden, D.C., Dixon, J.B., and Chen, C.C. (1986) Ion exchange, thermal transformations, and oxidizing properties of birnessite. Clays and Clay Minerals, 34, 511–520.

Greaves, C. (1985) Rietveld analysis of powder neutron diffraction data displaying anisotropic crystallite size broadening. Journal of Applied Crystallography, 18, 48–50.

Guthrie, G.D. (1989) Transmission electron microscope study of fluid-rock interactions. Ph.D. dissertation, The Johns Hopkins University, Baltimore, Maryland.

Jones, L.H.P., and Milne, A.A. (1956) Birnessite, a new manganese oxide mineral from Aberdeenshire, Scotland. The Mineralogical Magazine, 31, 283–288.

Oscarson, D.W., Huang, P.M., and Liaw, W.K. (1981) The role of manganese in the oxidation of arsenite by freshwater lake sediments. Clays and Clay Minerals, 29, 219–225.

Post, J.E., and Appleman, D.E. (1988) Chalcophanite, $ZnMn_3O_7 \cdot 3H_2O$: New crystal-structure determinations. American Mineralogist, 73, 1401–1404.

Post, J.E., and Bish, D.L. (1988) Rietveld refinement of the todorokite structure. American Mineralogist, 73, 861–869.

Potter, R.M., and Rossman, G.R. (1979a) Mineralogy of manganese dendrites and coatings. American Mineralogist, 64, 1219–1226.

Potter, R.M., and Rossman, G.R. (1979b) The tetravalent manganese oxides: Identification, and structural relationships by infrared spectroscopy. American Mineralogist, 64, 1199–1218.

Shannon, R.D. (1976) Revised effective ionic radii and systematic studies of interatomic distances in halides and chalcogenides. Acta Crystallographica, A32, 751–767.

Stähli, E. (1968) Über Manganate(IV) mit Schichten-Struktur. Ph.D. dissertation, University of Bern, Bern, Switzerland.

Stewart, J.M., and Hall, S.R., Eds. (1985) The XTAL system of crystallographic programs. University of Maryland, College Park, Maryland.

Taylor, R.M., McKenzie, R.M., and Norrish, K. (1964) The mineralogy and chemistry of manganese in some Australian soils. Australian Journal of Soil Research, 2, 235–248.

Wadsley, A.D. (1955) The crystal structure of chalcophanite, $ZnMn_3O_7 \cdot 3H_2O$. Acta Crystallographica, 8, 165–172.

Manuscript received August 14, 1989
Manuscript accepted February 6, 1990